Chem

CellPress

Article

Selectivity Control in Photocatalytic Valorization of Biomass-Derived Platform Compounds by Surface Engineering of Titanium Oxide

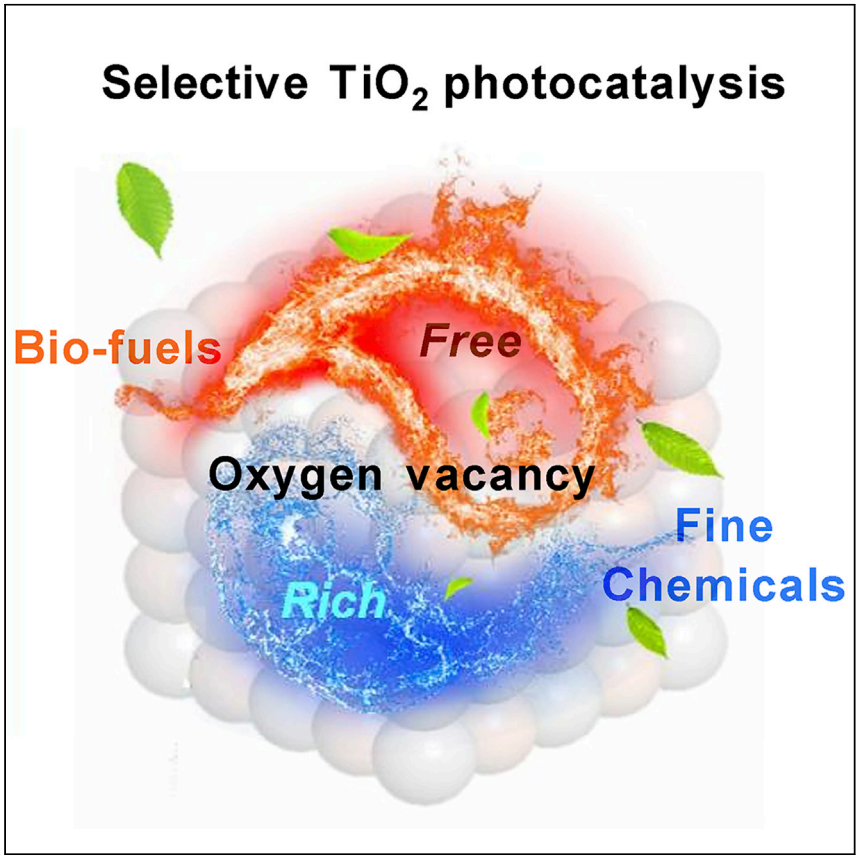

Wang and colleagues found that the selectivity for photocatalytic transformations of lignocellulose-derived platform chemicals including furfural, methyl furfural, and vanillin depended strongly on the exposed facet of TiO_2. They demonstrated that the facet-dependent density of oxygen vacancies governs the charge distribution and adsorption strength of surface species, and thus determines product selectivity. Hydrogenation products such as fine chemicals and coupling products as biofuel precursors can be produced in high yields over oxygen-vacancy-rich and oxygen-vacancy-free TiO_2 surfaces, respectively.

Xuejiao Wu, Jieqiong Li, Shunji Xie, ..., Qinghong Zhang, Jun Cheng, Ye Wang

zhangqh@xmu.edu.cn (Q.Z.)
chengjun@xmu.edu.cn (J.C.)
wangye@xmu.edu.cn (Y.W.)

HIGHLIGHTS

Selectivity for the reduction of bioplatforms depends on exposed facets of TiO_2

Coupling products as fuel precursors are produced in high yields

Surface-oxygen vacancies play pivotal roles in controlling the selectivity

Density of oxygen vacancies governs electronic structure of adsorbed species

Wu et al., Chem 6, 1–16
November 5, 2020
https://doi.org/10.1016/j.chempr.2020.08.014

Please cite this article in press as: Wu et al., Selectivity Control in Photocatalytic Valorization of Biomass-Derived Platform Compounds by Surface Engineering of Titanium Oxide, Chem (2020), https://doi.org/10.1016/j.chempr.2020.08.014

Chem

CellPress

Article

Selectivity Control in Photocatalytic Valorization of Biomass-Derived Platform Compounds by Surface Engineering of Titanium Oxide

Xuejiao Wu,[1,2] Jieqiong Li,[1,2] Shunji Xie,[1,2] Pengbo Duan,[1] Haikun Zhang,[1] Jun Feng,[1] Qinghong Zhang,[1,*] Jun Cheng,[1,*] and Ye Wang[1,3,*]

SUMMARY

Photocatalysis has offered a promising opportunity for selective transformation of biomass to high-value chemicals or fuels under mild conditions. Whereas titanium oxide has been widely used for photocatalytic pollutant degradation, H_2 evolution, and CO_2 reduction, few studies have been devoted to TiO_2-based photocatalytic valorization of biomass or biomass-derived platform compounds. Here, we report on surface-controlled photocatalysis of TiO_2 for selective valorization of furfurals and vanillin that are lignocellulose-derived key platform compounds. The reaction can be switched from hydrogenation of aldehyde group to C–C coupling by manipulating exposed facets; furanic and aromatic alcohols or coupling products, which are fine chemicals or jet-fuel precursors, could be produced with high selectivity. Our studies elucidate that the facet-dependent density of oxygen vacancies governs the charge distribution and adsorption strength of surface species and thus controls product selectivity. The present work offers an example of selectivity control by engineering TiO_2 surfaces for valorization of biomass-derived feedstocks.

INTRODUCTION

As one of the most popular photocatalysts, titanium dioxide (TiO_2) has triggered broad interest for decades and is still the focus of current intensive studies.[1] Besides strategies such as doping, sensitization, and heterojunction construction to facilitate the light absorption and charge-carrier separation, much recent attention has been paid to TiO_2 surface engineering, because the interfacial charge-transfer process, the substrate adsorption, activation, and reactions are dominated by surface properties.[2–4] For examples, anatase TiO_2 with high-energy {001} facet mainly exposed was successfully fabricated,[5] and the high-energy surface was found to favor the activity in a number of photocatalytic reactions.[3,6] However, so far only limited studies have been devoted to surface-dependent selectivity control in TiO_2 photocatalysis.[7] This is partially because TiO_2 has mainly been studied for pollutant degradation, H_2 evolution, and CO_2 reduction,[1–4,6–8] and most of the studies in these fields have been concerned more about activity than selectivity.

Recently, photocatalysis has shown great potential in the valorization of biomass or biomass-derived platform compounds (bioplatforms).[9,10] Thermocatalysis for biomass transformations usually requires harsh reaction conditions such as elevated temperatures and high pressures, which inevitably lead to undesirable side reactions and low selectivity of target products. In contrast, photocatalysis can be performed

The Bigger Picture

Photocatalysis has emerged as a useful approach to the sustainable production of value-added products from biomass, in which selectivity is the key issue because a number of transformations are possible when multifunctional biochemicals are the reactants. As one of the most popular photocatalysts, TiO_2 has mainly been applied to reactions like pollutant degradation that concern more about activity than selectivity. The knowledge about selectivity-controlling principles for TiO_2 is limited. Here, we report the first illustration of TiO_2-based photocatalysis that succeeds in modulating product selectivity in bioplatform transformations. Fine chemicals or jet-fuel precursors have been produced in high yields by controlling the density of oxygen vacancies on TiO_2, which governs surface adsorption and reaction and thus determines the product selectivity. This work offers useful insights into the design of selective photocatalysts for biomass valorization by surface engineering.

under mild conditions and thus is capable of avoiding side reactions. Further, photocatalysis has the potential to accomplish reactions that are difficult to realize by thermocatalysis owing to unique reaction mechanisms induced by photogenerated electrons and holes.[11] A few recent studies have utilized TiO_2 for photocatalytic oxidation of monosaccharides into the corresponding carboxylates or C_2–C_5 oxygenates.[12,13] However, the studies on TiO_2-catalyzed reductive transformations of bioplatforms, which play crucial roles in biomass valorization, are very scarce.[9,10] Therefore, the development of new photocatalytic systems for reductive valorization of bioplatforms using the cheap, stable, and environmental friendly TiO_2 would offer promising routes for sustainable production of high-value biobased chemicals and fuels under mild conditions.

Selectivity control is one of the most important issues in the valorization of bioplatforms because of multiple functional groups in bioplatform molecules and many possible reaction channels to different products. For example, furfural, methyl furfural, and vanillin are key feedstocks easily produced from lignocellulosic biomass (Scheme S1),[14–16] and the reductive transformations of these bioplatform molecules can offer both furanic and aromatic primary alcohols, which are important fine chemicals in the fragrance and resin industries, as well as C–C coupling products with 10–18 carbons, which are potential precursors for high-quality diesel or jet fuel (Figure 1).[17] In addition, reactions such as hydrogenation of furanic/aromatic rings or decarbonylation may also take place under thermocatalytic conditions. It is noteworthy that the selective production of fuel precursors by homo-coupling or cross-coupling of bioplatforms is particularly difficult by thermocatalysis and only very limited success has been achieved in spite of the significance of this type of reactions.[18,19] Reductive coupling of bioplatforms with high selectivity remains one of the most challenging goals in biomass valorization.

Here, we report that TiO_2 nanocrystals efficiently catalyze photoreductive transformations of furfurals and vanillin, two types of important bioplatforms, into corresponding alcohols and coupling products under mild conditions. We discovered that the selectivity toward hydrogenation of aldehyde group to alcohols or reductive coupling to coupling products can be easily controlled by engineering exposed facets of TiO_2 nanocrystals. We uncovered that the facet-controlled selectivity is determined by the density of surface-oxygen vacancies generated *in situ*. Different reaction mechanisms in the presence and absence of surface-oxygen vacancies have been elucidated on the molecular level. To the best of our knowledge, this is the first example of success in modulating product selectivity in photocatalytic reductive transformations of bioplatforms and in the achievement of high yields of coupling products. The present work would inspire the design of photocatalytic systems for biomass valorization with controlled reaction pathways and product selectivity through surface engineering of semiconductor catalysts.

RESULTS

Furfural Conversion over TiO_2 with Different Facets

We fabricated three types of TiO_2 nanocrystals with different morphologies and exposed facets (Figure S1), including bipyramid-shaped anatase with {101} facets mainly exposed (denoted as A-bipyramid), anatase nanosheet dominated by {001} facets (denoted as A-sheet), and rod-shaped rutile enclosed mainly by {110} facets (denoted as R-rod). Photocatalytic conversion of furfural over the A-bipyramid, the most available anatase TiO_2 nanocrystal,[3] has been investigated in detail. No product was observed without light irradiation or in the absence of catalyst. Furfural

[1]State Key Laboratory of Physical Chemistry of Solid Surfaces, Collaborative Innovation Center of Chemistry for Energy Materials, National Engineering Laboratory for Green Chemical Productions of Alcohols, Ethers and Esters, College of Chemistry and Chemical Engineering, Xiamen University, Xiamen 361005, China

[2]These authors contributed equally

[3]Lead Contact

*Correspondence: zhangqh@xmu.edu.cn (Q.Z.), chengjun@xmu.edu.cn (J.C.), wangye@xmu.edu.cn (Y.W.)

https://doi.org/10.1016/j.chempr.2020.08.014

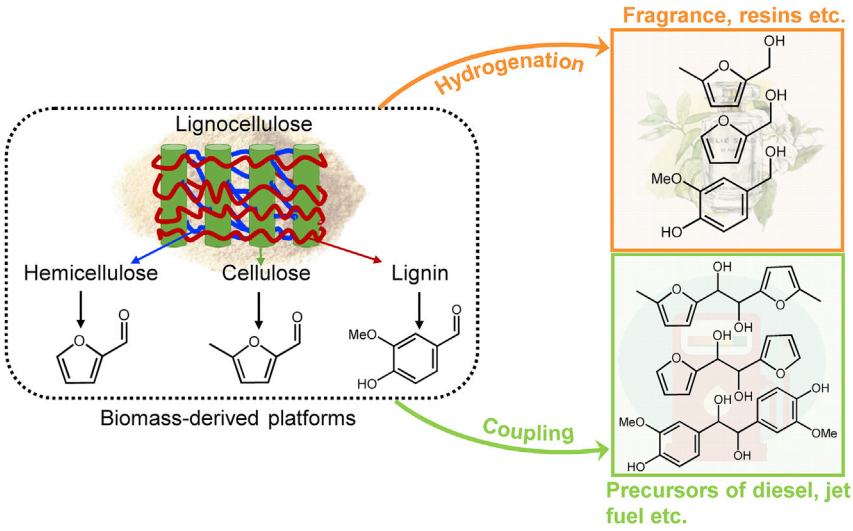

Figure 1. Transformations of Lignocellulose-Derived Platforms

Furfural, 5-methyl furfural, and vanillin can be derived from hemicellulose, cellulose, and lignin, which are three major components of lignocellulosic biomass, respectively.

alcohol, a product by hydrogenation of the aldehyde group, as well as hydrofuroin and furoin, which could be formed by reductive coupling of furfural (Figures 2A and S2), were formed over the A-bipyramid (Figure 2B). We adopted $mmol_{furanic\ ring}\ g^{-1}$ as the unit of the yield of each product, and it is noteworthy that one mole of hydrofuroin or furoin contains two moles of furanic ring. Formaldehyde was also formed in a considerable amount (Table S1; Figure S2F). The analysis of the reactions induced by photogenerated electrons and holes suggests that furfural undergoes both aldehyde-group hydrogenation to furfural alcohol and reductive coupling to hydrofuroin and furoin by photogenerated electrons on the A-bipyramid, whereas formaldehyde is the product from methanol, the solvent, by photogenerated holes (Table S1; Scheme S2). We found that the reaction completely stopped when the solvent was changed from methanol to a proton-free solvent, e.g., acetonitrile. The intentional addition of Na_2S/Na_2SO_3 (4 mM Na_2S + 2 mM Na_2SO_3) as sacrificial agents to help the consumption of holes could not cause the formation of reduction products with acetonitrile solvent. These findings indicate that methanol also functions as the proton source in combination with photogenerated electrons for the reductive transformation of furfural (Scheme S2). Using methanol, a cheap solvent that can be derived from biomass,[20] as the hydrogen donor can avoid the use of high-pressure H_2 or corrosive formic acid, rendering the current process safe and environmentally friendly.[21,22]

The selectivity of products strongly depended on the exposed facet. Unlike the A-bipyramid, the A-sheet was highly selective toward the hydrogenation of aldehyde group, offering furfural alcohol as the dominant product with a selectivity reaching 90% after a 4-h reaction (Figure 2C). On the other hand, the R-rod was very specific for the formation of coupling products, i.e., hydrofuroin and furoin, and the formation rate of coupling products reached 32 $mmol_{furanic\ ring}\ g^{-1}\ h^{-1}$ with nearly 100% selectivity (Figure 2D).This rate is more than twice that reported over a Ru-doped $ZnIn_2S_4$ photocatalyst, which showed a formation rate of 13 $mmol_{furanic\ ring}\ g^{-1}h^{-1}$ for coupling products in the photocatalytic conversion of methylfurans that could be produced from furfurals by further hydrodeoxygenation.[23] Further, as compared with some typical thermocatalytic systems for furfural reduction (Table

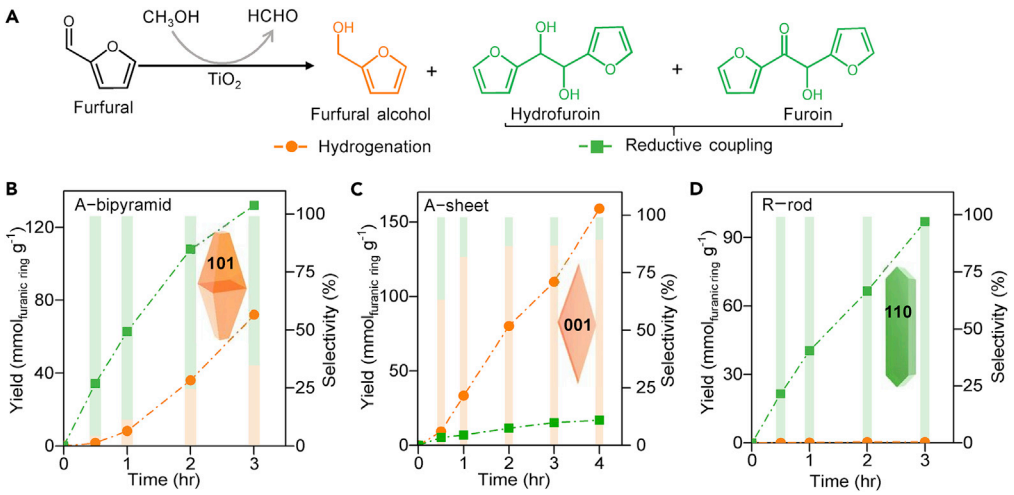

Figure 2. Photocatalytic Conversion of Furfural over TiO_2 Nanocrystals

(A) Structures of products from hydrogenation of aldehyde group and reductive coupling of furfural.

(B) Changes of product yield and selectivity with time over A-bipyramid.

(C) Changes of product yield and selectivity with time over A-sheet.

(D) Changes of product yield and selectivity with time over R-rod. The yields of products is presented in $mmol_{furanic\ ring}\ g_{catalyst}^{-1}$. Note that 1 mole of hydrofuroin or furoin contains 2 moles of furanic ring. The inset models show the morphologies of TiO_2 with the mainly exposed facet.

S2), the present TiO_2-based photocatalytic system showed better activity under mild conditions. Moreover, the by-products that are usually formed in thermocatalysis such as tetrahydrofurfuryl alcohol by hydrogenation of furanic rings and furan by decomposition of aldehyde groups have not been observed in our system. The mild reaction conditions may contribute to the perseveration of valuable functional groups. Therefore, the present simple TiO_2-based photocatalytic system is very promising for valorization of furfural, and in particular, not only furfural alcohol but also reductive coupling products can be formed with high selectivity and a high formation rate.

It is noteworthy that while the yield of coupling products increased almost linearly with reaction time from the beginning (Figure 2D), the formation of furfural alcohol proceeded quite slowly in the initial stage (< 0.5 h) and then accelerated after an induction period over both the A-bipyramid and A-sheet (Figures 2B and 2C). The selectivities of furfural alcohol were 4.6% and 63% at a reaction time of 0.5 h for A-bipyramid and A-sheet, respectively, and they increased significantly to 35% and 87% after 3 h of reaction (Figures 2B and 2C). The existence of induction period for the formation of furfural alcohol suggests the evolution of surface structures of the A-bipyramid and A-sheet during the reaction.

Characterizations and Structure-Performance Relationship

The band-gap energies of A-sheet, A-bipyramid, and R-rod before reaction estimated from UV-vis diffuse reflectance spectra (Figure 3A) were 3.24, 3.22, and 3.03 eV, respectively. These values are consistent with the band-gap energies of anatase (~3.2 eV) and rutile (~3.0 eV) TiO_2.[1] The UV-vis spectra for the A-sheet and A-bipyramid catalysts after photocatalytic reactions showed shifts of absorption edges to longer wavelengths corresponding to band-gap narrowing and additional absorption tails extending to the visible-light region (Figure 3A). This observation corresponded well to the change in color from white to grayish blue for these two catalysts after reaction.[24,25] The band-gap narrowing and UV-vis spectrum-tailing phenomena may be contributed by the generation of oxygen vacancies (V_O)[26] or

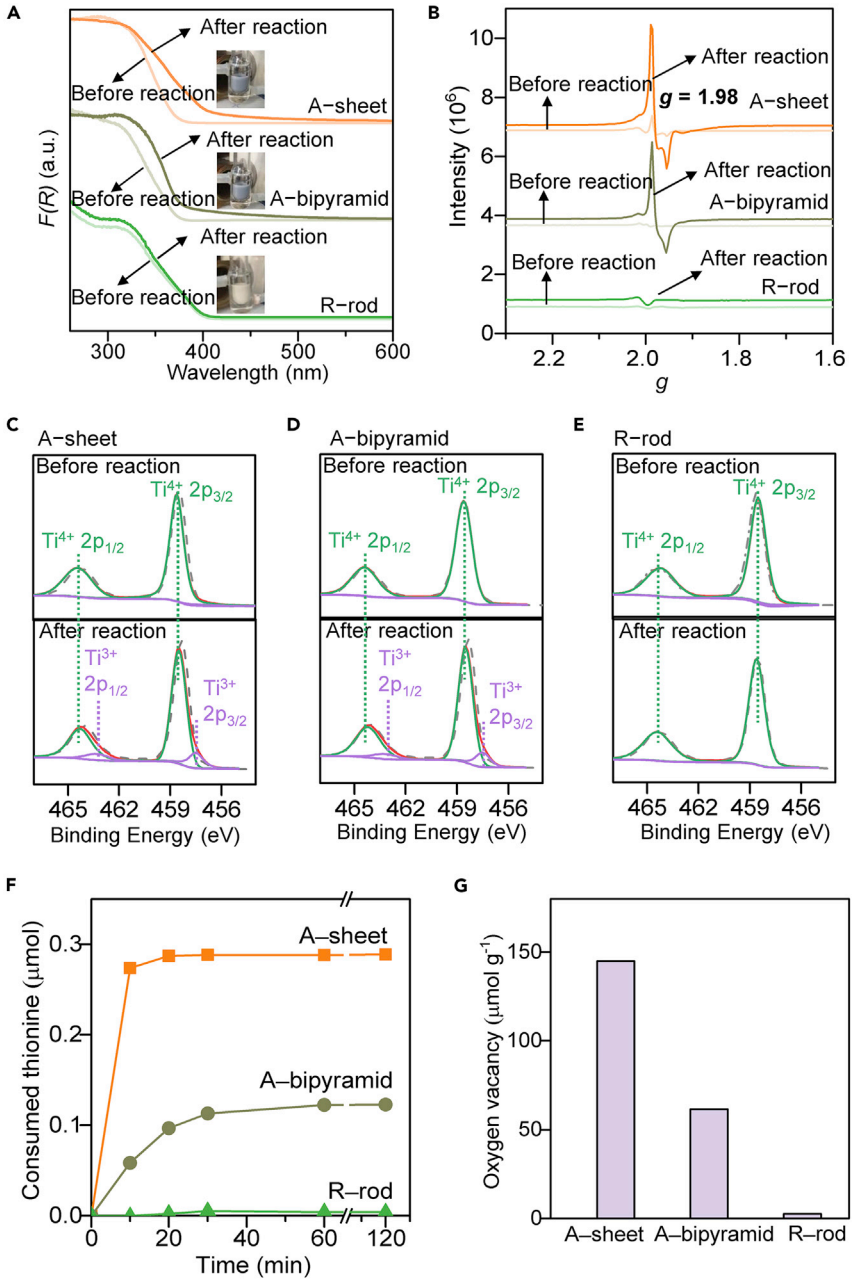

Figure 3. Characterizations of TiO_2 Nanocrystals

(A) UV-visible diffuse reflectance spectra. The inset pictures show the color of TiO_2 after photocatalytic reaction.

(B) Low-temperature EPR spectra measured at 77 K.

(C) Ti 2p XPS spectra for A-sheet.

(D) Ti 2p XPS spectra for A-bipyramid.

(E) Ti 2p XPS spectra for R-rod.

(F) Consumption of thionine versus photo-irradiation time.

(G) Density of oxygen vacancies.

structural disorders[27] on the A-sheet and A-bipyramid. The irradiation of TiO_2 in methanol, the solvent, may create surface V_O sites (Scheme S3).[28] In contrast, the UV-vis spectrum and color of the R-rod did not undergo significant changes after

Please cite this article in press as: Wu et al., Selectivity Control in Photocatalytic Valorization of Biomass-Derived Platform Compounds by Surface Engineering of Titanium Oxide, Chem (2020), https://doi.org/10.1016/j.chempr.2020.08.014

the photocatalytic reaction. Electron paramagnetic resonance (EPR) and X-ray photoelectron spectroscopy (XPS) measurements provided further evidence for the presence of V_O on the A-sheet and A-bipyramid and the absence of V_O on the R-rod after reaction. EPR measurements performed at 77 K showed a signal at g value of 1.98, which could be ascribed to Ti^{3+} in TiO_2,[29] for the A-sheet and A-bipyramid after photocatalytic reaction, whereas this signal was insignificant for the used R-rod catalyst (Figure 3B). It is widely accepted that Ti^{3+} is a charge-compensation species accompanying the appearance of V_O sites on TiO_2.[30] While not distinct, a weak signal at g = 2.01 also appeared. EPR measurements conducted at 298 K for the catalysts after photocatalytic reactions showed a decrease in the intensity of signal at g = 1.98, which is assignable to Ti^{3+}, whereas the signal at g = 2.01 became significantly stronger for the A-sheet and A-bipyramid (Figure S3). The change in EPR spectra may result from the interaction of O_2 with the surface Ti^{3+} and V_O site, forming O^- on the surface at the expense of Ti^{3+}.[31] The Ti 2p core-level spectra obtained by XPS for the A-sheet or A-bipyramid before reaction were dominated by peaks at 458.6 and 464.4 eV, assignable to Ti $2p_{3/2}$ and Ti $2p_{1/2}$ of Ti^{4+}, whereas two shoulders at 457.4 and 463.1 eV, attributable to those of Ti^{3+} accompanying the surface V_O sites, appeared after reactions (Figures 3C and 3D).[32,33] On the other hand, no significant differences in Ti 2p spectra for the R-rod catalyst before and after reactions were observed (Figure 3E). The O 1s XPS results for all the samples exhibited two peaks; the peak at 529.7 eV could be ascribed to the lattice oxygen, while that at 531.5 eV was assignable to the Ti-OH species or defective oxygen species associated with V_O sites.[32,34] No significant differences were observed in the O 1s spectra before and after reactions (Figure S4). This is possibly because the V_O density is low and the peak at 531.5 eV may mainly be contributed by the Ti-OH species. Therefore, these characterization results demonstrate the generation of V_O sites on the A-sheet and A-bipyramid but not on the R-rod during the photocatalysis.

We have measured the surface V_O sites quantitatively by electron titration with thionine, the consumption of which corresponds to the amount of electrons trapped in V_O sites.[35] While the consumption of thionine over the R-rod irradiated with different times was negligible, considerable amounts of thionine were consumed over the A-sheet and A-bipyramid (Figure 3F). The consumption of thionine was faster over the A-sheet than over the A-bipyramid in the initial stage, suggesting that the V_O site was easier to form on the A-sheet under light irradiation. The density of V_O sites evaluated from the consumption of thionine decreased in the order of A-sheet (145 μmol g^{-1}) > A-bipyramid (61.5 μmol g^{-1}) > R-rod (2.52 μmol g^{-1}) (Figure 3G).

In short, our characterizations suggest that the V_O can be generated on catalyst surfaces during photocatalytic conversion of furfural in methanol and the density of V_O sites depends on the exposed facets, decreasing in the order of anatase {001} > anatase {101} > rutile {110}. This trend is in agreement with the surface energy of these facts.[2–4] As displayed in Scheme S3, we propose that the V_O site is generated through the stoichiometric reaction between methanol and TiO_2. It should be noted that the density of V_O sites and the amount of methanol consumed for the generation of V_O sites are remarkably lower than the amounts of furfural alcohol formed in the hydrogenation of aldehyde group of furfurals. The yields of furfural alcohol were 72 and 152 mmol g^{-1} over the A-bipyramid and A-sheet with V_O densities of 61.5 and 145 μmol g^{-1} during the photocatalytic conversion of furfural for 3 and 4 h, respectively (Figures 2B and 2C). The turnover numbers for furfural alcohol formation per V_O site are both >1,000 over the A-bipyramid and A-sheet. Therefore, the reduction of furfural to furfural alcohol proceeds catalytically over the V_O site. We

Please cite this article in press as: Wu et al., Selectivity Control in Photocatalytic Valorization of Biomass-Derived Platform Compounds by Surface Engineering of Titanium Oxide, Chem (2020), https://doi.org/10.1016/j.chempr.2020.08.014

further confirmed that the catalyst could be used repeatedly. Recycling tests of the A-bipyramid for photocatalytic conversion of furfural showed only a slight change in performance in the second cycle, and the performance could almost be sustained in the third and fourth cycles (Figure S5).

The structure-performance correlation suggests that the surface V_O site plays a crucial role in aldehyde-group hydrogenation, whereas the V_O-free TiO_2 surface is responsible for the coupling reaction. It is noteworthy that the density of V_O sites mainly determines the selectivity, and the activity may be influenced by many factors such as the light absorption, the ability of photogenerated electron-hole separation and the surface reaction. For the series of A-bipyramid, A-sheet, and R-rod catalysts, the light absorption (Figure 3A) and the ability of electron-hole separation as reflected by the photocurrent density (Figure S6) do not have big differences. We found that the specific surface areas of this series of catalysts, which may influence the catalytic performance, are quite different (Table S3). We speculate that the larger surface area of the A-bipyramid results in its higher yield of coupling products as compared with the R-rod (Figure 2), although the selectivity of coupling products is lower over the A-bipyramid than that over the R-rod.

We further studied the commercial TiO_2 (Degussa P25) for the photocatalytic conversion of furfural. Furfural alcohol and coupling products (hydrofuroin and furoin) were formed with selectivities of 19% and 81%, respectively (Figure S7). The surface V_O density measured by electron titration was 34 μmol g^{-1} for P25, and thus the V_O density increased in the sequence of R-rod < P25 < A-bipyramid < A-sheet. It is of interest that both the selectivity and the yield of furfural alcohol change in the same order (Figure S7; Table S3). On the other hand, the selectivity of coupling products decreased in the sequence of R-rod > P25 > A-bipyramid > A-sheet, confirming that the V_O-free TiO_2 surface plays a crucial role in the formation of coupling products. However, the yield of coupling products based on specific surface area over P25 was relatively lower than that over the A-bipyramid. This is probably because of the lower ability of P25 in electron-hole separation (Figure S6). We further prepared P25-based TiO_2 samples with increased V_O densities by treatment with $NaBH_4$, a strong reductant that is known to be capable of creating surface V_O sites on TiO_2 under mild conditions.[36] The catalysts denoted as P25-0.5, P25-0.75, and P25-1, which had almost the same specific surface area (51–55 m^2 g^{-1}), were obtained by treating P25 with different concentrations of $NaBH_4$ aqueous solutions. It is of interest that both the furfural alcohol selectivity (Figure S7B) and the surface V_O density (Figure S7C) increased with the concentration of $NaBH_4$. This result provides further evidence that the V_O site favors the hydrogenation of aldehyde group of furfural to furfural alcohol. However, the yield of total products per either catalyst weight or surface area for the P25-1 catalyst with the highest V_O density rather decreased (Figure S7D). This is possibly because of the decreased electron-hole separation ability of this deeply reduced catalyst (Figure S7E).

DFT Calculations and Roles of Oxygen Vacancies

To understand the role of V_O sites in determining the reaction channel, we performed density functional theory (DFT) calculations for the conversion of furfural on catalyst surfaces with and without V_O. The optimized geometries indicate a tilted η^1-(O) configuration of furfural adsorbed on both V_O-free and V_O-rich surfaces (Figures S8 and S9). As compared with other adsorption modes, the η^1-(O) adsorption mode, with the carbonyl oxygen bound to Ti cation and the furan ring repulsed away from the surface, is beneficial to the selective activation of aldehyde group.

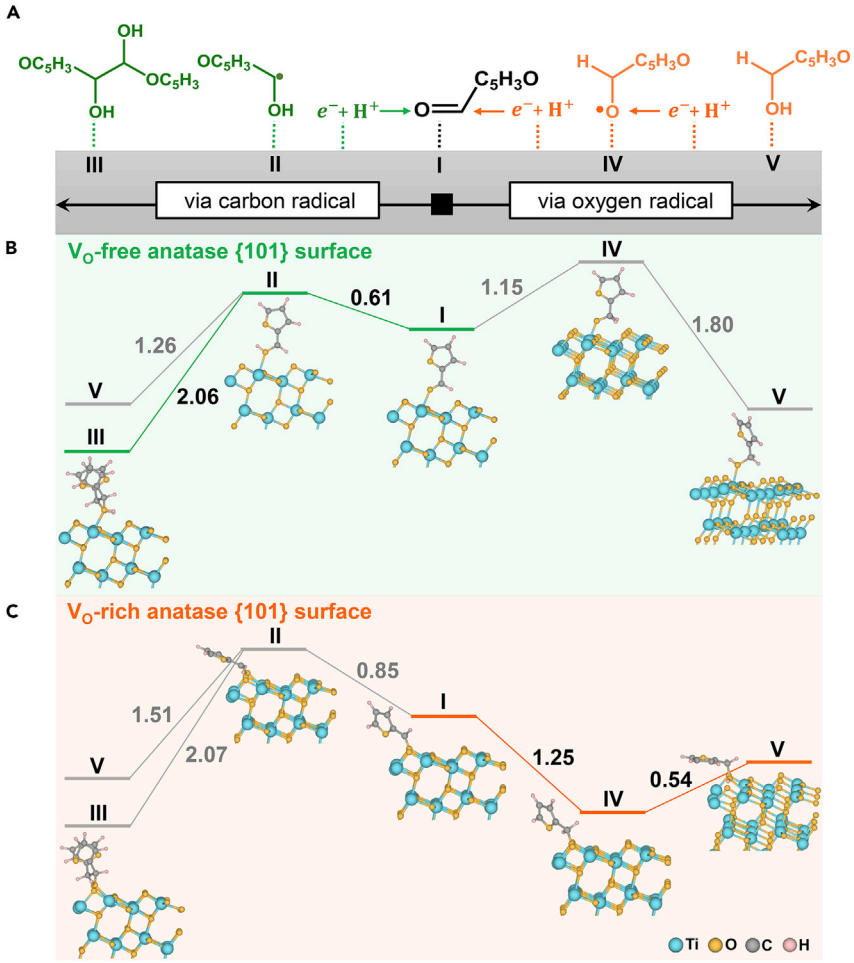

Figure 4. DFT Calculations for Furfural Conversion on TiO_2

(A) Reaction pathways of hydrogenation of aldehyde group and reductive coupling.

(B) Total-energy-change profiles for furfural reduction on V_O-free anatase {101} surface.

(C) Total-energy-change profiles for furfural reduction on V_O-rich anatase {101} surface.

For example, the η^2-(C,O) configuration would cause the decarboxylation or hydrogenation of the furan ring.[37]

Generally, for photocatalytic reduction, electron and proton transfer may occur not only through stepwise proton transfer followed by electron transfer (PT-ET)[38] or electron transfer followed by proton transfer (ET-PT)[39] but also through a concerted proton-electron transfer (CPET)[40–42] manner (Figure S10). We have studied the reaction mechanism with a total-energy-change approach (the energy difference between product and reactant), regardless of the detailed proton-electron transfer process. Therefore, the above transfer mechanisms are uniformly expressed as (e^- + H^+) transfer hereafter. Two possible reduction pathways exist for the hydrogenation of adsorbed furfural in the first step (Figure 4A): (1) the addition of (e^- + H^+) to the O atom of the carbonyl group, resulting in the formation of a C radical (·C–OH) (I→II); and (2) the addition of (e^- + H^+) to the C atom of the carbonyl group, leading to an O radical (CH–O·) (I→IV). In the second step, the ·C–OH intermediate may either be coupled with a second C radical to produce hydrofuroin (II→III) or be further reduced by the addition of (e^- + H^+) to form furfural alcohol (II→V). The

Please cite this article in press as: Wu et al., Selectivity Control in Photocatalytic Valorization of Biomass-Derived Platform Compounds by Surface Engineering of Titanium Oxide, Chem (2020), https://doi.org/10.1016/j.chempr.2020.08.014

CH–O· intermediate can only result in furfural alcohol by addition of another (e^- + H^+) (IV → V).

The DFT calculation reveals that on the V_O-free anatase {101} surface, the hydrogenation energy for the attack of (e^- + H^+) to O atoms of carbonyl to form the ·C-OH intermediate (I → II) is 0.61 eV, which is more favorable by 0.54 eV than the hydrogenation through the attack of (e^- + H^+) to the C atom of carbonyl (Figure 4B). The ·C–OH subsequently undergoes coupling with an energy decrease of 2.06 eV (II → III), which is more favorable than the hydrogenation by 0.8 eV. In contrast, on the V_O-rich anatase {101} surface, the formation of CH–O· (I → IV) is an exothermic reaction, whereas the formation of ·C–OH (I → II) is endothermic (Figure 4C), and thus, furfural prefers to undergo a two-step hydrogenation mechanism to furfural alcohol. Similar conclusions have been obtained on the V_O-free and V_O-rich anatase {001} (Figure S11) as well as V_O-free and V_O-rich rutile {110} surfaces (Figure S12). Therefore, our DFT calculations on the energetics of reaction pathways have confirmed the experimental findings that the presence of V_O on TiO_2 surfaces favors the hydrogenation of aldehyde group in furfural, whereas coupling products are formed preferentially on V_O-free surfaces.

Further DFT calculations were performed to gain in-depth insights into the difference in selectivity on the V_O-free and V_O-rich TiO_2 surfaces. For the V_O-free surface, the charge-difference analysis reveals that there is no significant charge transfer between TiO_2 and furfural (green panel in Figure 5A). Instead, a small amount of charge rearrangement occurs inside furfural molecules (Figure S13A). Because of the higher electronegativity of O, the O and C atoms of carbonyl are negatively and positively charged, respectively (green panel in Figure 5B). Thus, the O atom of carbonyl is more favorably hydrogenated, leading to the ·C–OH intermediate. On the other hand, when furfural is adsorbed on the V_O-rich TiO_2 surface via the filling of the V_O site by the O atom of carbonyl, a significant charge transfer occurs from the two Ti^{3+} ions neighboring to the V_O site to furfural (orange panel in Figure 5A; Figure S13B). The charge redistribution may induce negative charges around the C atom of carbonyl group (orange panel in Figure 5B). Moreover, the embedded carbonyl O atom is coordinatively saturated by Ti, and consequently the (e^- + H^+) is preferably bound to the C atom of carbonyl group to form the CH–O· intermediate (orange panel in Figure 5B; Table S4). Furthermore, the calculation reveals that the C radical formed on the V_O-free surface has a much smaller adsorption energy than the O radical formed on the V_O-rich surface (Figure 5C; Table S5). Thus, the C radical may readily desorb from the V_O-free TiO_2 surface and dimerizes to form the coupling products, whereas the strongly bound O radical on the V_O-rich surface preferably undergoes consecutive (e^- + H^+) addition to yield furfural alcohol.

Therefore, our calculations indicate that the product selectivity in furfural conversion on the V_O-free and V_O-rich surfaces is determined by the interaction between the reactant and the surface. The electron transfer between the TiO_2 surface and furfural molecule controls the preferential attack of (e^- + H^+) onto C or O atom in a carbonyl group, leading to the formation of O or C radical intermediate and different types of products. The strength of adsorption of reaction intermediate on TiO_2 surfaces also affects the product selectivity.

Experiments were performed to probe the interaction of the reactant with the V_O-rich and V_O-free surfaces. Because rich V_O and almost no V_O sites were generated *in situ* on the A-sheet and R-rod, respectively, these two catalysts were chosen to represent the V_O-rich and V_O-free surfaces in our experiments. The transient

Please cite this article in press as: Wu et al., Selectivity Control in Photocatalytic Valorization of Biomass-Derived Platform Compounds by Surface Engineering of Titanium Oxide, Chem (2020), https://doi.org/10.1016/j.chempr.2020.08.014

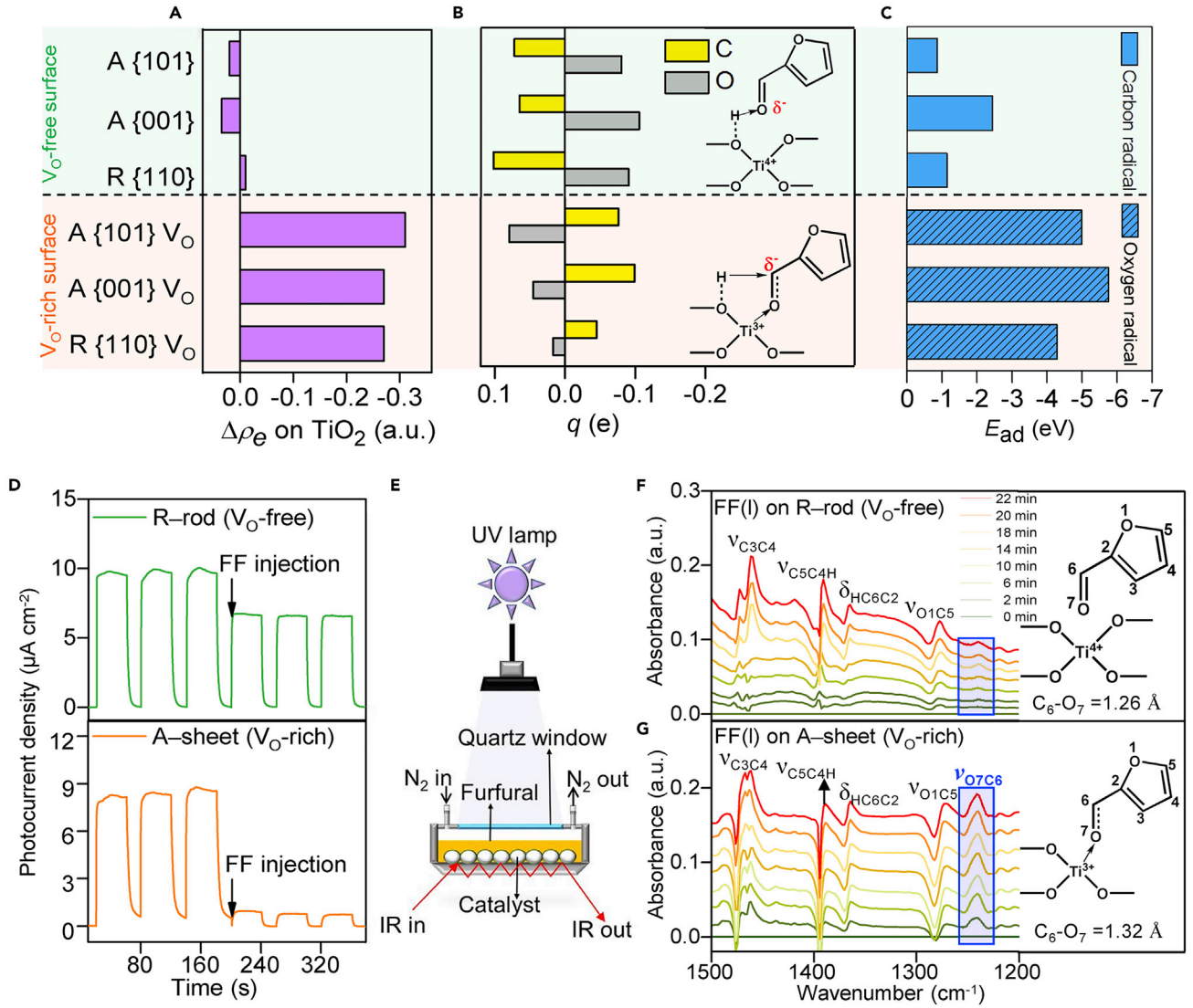

Figure 5. Interactions between Furfural and TiO_2 Surfaces

(A) Electron density changes ($\Delta\rho_e$) on TiO_2 before and after furfural adsorption.

(B) Hirshfeld charge distributions in carbonyl C and O atoms. Right panel: preferential attack behavior of H atom onto carbonyl C or O atom.

(C) Adsorption energies (E_{ad}) of C radical on V_O-free surfaces and O radical on V_O-rich surfaces.

(D) Transient photocurrent responses of R-rod and A-sheet before and after furfural (FF) injection.

(E) Schematic setup for ATR-FTIR spectroscopy. N_2 is the protecting gas to prevent ATR-FTIR measurements from the influence of air.

(F) Time-resolved ATR-IR spectra of furfural on R-rod.

(G) Time-resolved ATR-IR spectra of furfural on A-sheet. The V_O-free and V_O-rich surfaces in (A), (B), and (C) include anatase {101}, anatase {001} and rutile {110} surfaces. The chemical structures and bonding length of carbonyl group on V_O-free surface of rutile {110} and V_O-rich surface of anatase {001} are displayed on the right panels of (F) and (G).

photocurrent response study was performed in methanol, i.e., the solvent, and the electrode with photocatalyst was illuminated under UV light for 1 h before measurement. This pretreatment generated V_O sites with saturated concentrations on the A-sheet and R-rod surfaces. The result for the R-rod showed a slight difference in the presence and absence of furfural, suggesting a weak interaction between furfural and the V_O-free surface (Figure 5D). In contrast, a big decrease in the photocurrent density was observed after the injection of furfural onto the A-sheet, indicating that the interfacial electron transfer induced a strong interaction between the V_O-rich

surface and furfural.[43] Transient photocurrent response measurements were also performed by using CH_3CN as the electrolyte without pretreatment of the photocatalyst, and thus the V_O density on catalyst surfaces would be very low. The result showed that the decrease in photocurrent density after the injection of furfural was not big not only for the R-rod but also for the A-sheet catalyst (Figure S14). The phenomenon that the photocurrent density only decreases slightly after furfural injection in the case of CH_3CN is similar to that for the R-rod with catalyst pretreatment in methanol (Figure 5D). This agrees with the finding that the density of V_O sites was low on the R-rod catalyst under irradiation in methanol.

Attenuated total reflection Fourier-transform infrared (ATR-FTIR) spectroscopy (Figure 5E), which could provide liquid-phase IR spectra of molecules on solid catalyst surfaces,[44] typically provides IR bands of furfural in a wavenumber region of 1,500–1,200 cm^{-1} (Table S6).[45,46] The thermogravimetric-differential thermal analysis (TG-DTA) showed that no organic adsorbates were present on catalyst surfaces before adsorption (Figure S15). Our time-resolved ATR-FTIR spectra recorded for the furfural-adsorbed R-rod and A-sheet both exhibited characteristic signals assignable to furfural (Figures 5F and 5G). Furthermore, an additional band centered at around 1,241 cm^{-1} was observed for the A-sheet, which could not be observed for the R-rod (Figures 5F and 5G). This new IR band could be assigned to the red-shift of carbonyl group caused by the strong interaction with the V_O-rich surface.[47] Our DFT calculations further revealed that for furfural on the V_O-free rutile {110} surface, the bond length of C=O (1.26 Å) had negligible change with respect to that in the gas phase (1.23 Å). However, on the V_O-rich anatase {001} surface, the C=O bond length for adsorbed furfural increased to 1.32 Å (Table S7), indicative of the change of C=O to C–O bond. The new IR band of adsorbed furfural on the V_O-rich surface may arise from the C–O stretching vibration for furfuryl-oxy adsorption state (Figure 5G). The appearance of this band further confirms the strong interaction and electron transfer between furfural and the V_O-rich surface.

The addition of a small amount of H_2O_2, a radical scavenger, into the system significantly suppressed the conversion of furfural over the A-sheet and R-rod (Table S8), confirming that both the hydrogenation and coupling reactions proceeded via radical intermediates. The formation of ·C–OH radical over the R-rod was further verified by the addition of 1,1-diphenylethylene as a radical trap.[48] A new compound with a mass-to-charge ratio (*m/z*) of 276, which could be assigned to the adduct of ·C–OH radical and 1,1-diphenylethylene, was detected in the product mixture (Figure S16). The adduct of CH–O· radical and 1,1-diphenylethylene, which should have fingerprint peaks of *m/z* at 97, 167, 181, and 278, could not observed for the A-sheet. This is probably because of the strong adsorption of CH–O· on V_O-rich surfaces (Figure 5C).

Valorization of Other Bioplatforms

Besides furfural, which can be easily obtained from hemicellulose, we have performed photocatalytic conversions of other bioplatforms derived from lignocellulosic biomass, including 5-methyl furfural from cellulose and vanillin from lignin, using the A-sheet and R-rod, which represent V_O-rich and V_O-free TiO_2 catalysts, respectively. The A-sheet was highly selective toward the hydrogenation of aldehyde group in these bioplatforms to form the corresponding alcohols (Figure 6), which are versatile fine chemicals. On the other hand, the R-rod exhibited unique selectivity toward the formation of coupling products and the yield of the corresponding coupling products reached $\geq$ 80%. These results demonstrate the

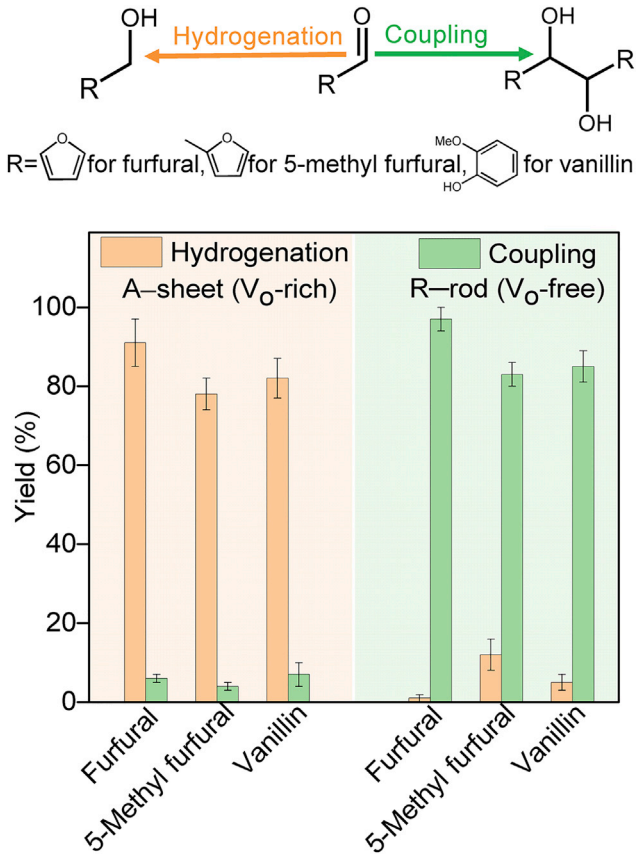

Figure 6. Photocatalytic Conversions of Bioplatforms

Furfural, 5-methyl furfural, and vanillin can be derived from hemicellulose, cellulose, and lignin, the three major components of lignocellulosic biomass, respectively. The experiments in each case were performed at least for three times. The error bar represents the absolute deviation, which is within 10%.

feasibility of TiO_2 surface engineering in tuning the selectivity in photocatalytic transformation of lignocellulosic biomass-derived platforms.

Surface defects like V_O sites, even in a low density, have the potential to regulate the surface electronic structure of semiconductors and thus can tune adsorbed chemicals and catalytic performance.[49,50] The interaction between the functional groups in reactants or intermediates and the catalyst surface is known to play a key role in determining the selectivity in thermocatalytic transformations of multifunctional chemicals.[14] However, how the surface defect functions in photocatalytic valorization of biomass is less understood. The present work contributes to presenting a first example to illustrate that the surface engineering by tuning the density of oxygen vacancies can successfully control the selectivity in photocatalytic transformation of multifunctional bioplatforms.

Conclusion

We discovered that TiO_2 is an efficient photocatalyst for the reductive transformation of lignocellulose-derived furfurals and vanillin and that surface-oxygen vacancies play a decisive role in determining the product selectivity. The catalyst without surface-oxygen vacancies favors the reductive coupling reaction to form

Please cite this article in press as: Wu et al., Selectivity Control in Photocatalytic Valorization of Biomass-Derived Platform Compounds by Surface Engineering of Titanium Oxide, Chem (2020), https://doi.org/10.1016/j.chempr.2020.08.014

C_{10}–C_{18} products, which are high-quality fuel precursors, whereas the catalyst with rich surface-oxygen vacancies preferentially catalyzes the hydrogenation of aldehyde group to form aromatic and furanic alcohols as versatile fine chemicals. High yields of the coupling products or aromatic and furanic alcohols have been achieved. Our mechanistic studies revealed that the density of oxygen vacancies affects the reactant-surface interaction and the charge transfer. The strong interaction between the oxygen-vacancy-rich surface and furfural leads to the preferential formation of CH–O· intermediate, and the strong adsorption of intermediate facilitates the subsequent addition of a second H atom to form furfural alcohol. On the other hand, the ·C–OH intermediate is formed on the oxygen-vacancy-free surface and the weak adsorption of the radical intermediate enables easy desorption and the subsequent C–C coupling. The present work not only demonstrates that surface-controlled TiO_2 is a promising photocatalyst for biomass valorization but also offers an opportunity to control the reaction pattern and product selectivity in transformation of multifunctional chemicals.

EXPERIMENTAL PROCEDURES

Resource Availability

Lead Contact

Further information and requests for resources and reagents should be directed to and will be fulfilled by the Lead Contact, Professor Ye Wang (wangye@xmu.edu.cn).

Materials Availability

This study did not generate new unique reagents.

Data and Code Availability

The published article includes all datasets generated or analyzed during this study.

Synthesis of TiO_2 Nanocrystals with Controlled Facets

To synthesize anatase TiO_2 with bipyramid morphology and {101} facet mainly exposed, titanium isopropoxide (20 mL) was mixed with distilled water (2 mL) in a Teflon autoclave. The mixture was then placed in an electric oven and held at 180°C for 36 h. After cooling to room temperature, the sample was separated by centrifugation, washed with distilled water and ethanol, dried overnight at 60°C, and calcined in air at 500°C for 3 h.[51] For the synthesis of anatase TiO_2 sheets dominated by {001} facet, tetrabutyl titanate (25 mL) was mixed with 47% hydrofluoric acid solution (3 mL) and the mixture was kept at 180°C for 24 h. After cooling to room temperature, the sample was separated by centrifugation, washed with 1 M NaOH, distilled water and ethanol, and dried overnight at 60°C.[52] For the synthesis of rutile TiO_2 rod enclosed mainly by {110} facet, tetrabutyl titanate (10 mL) was mixed with distilled water (10 mL) and 38% hydrochloric acid (10 mL), and the mixture was kept at 180°C for 24 h. After cooling to room temperature, the sample was separated by centrifugation, washed with 1 M NaOH, distilled water and ethanol, dried overnight at 60°C, and calcined in air at 500°C for 3 h.[53]

Evaluation of Photocatalytic Performance

For the conversion of furfural, TiO_2 (5 mg), furfural (100 μL, 1.2 mmol) and solvent (CH_3OH, 5 mL) were added into a quartz reactor (10 mL). The reactor was evacuated and purged with N_2 for 5 min. The reaction mixture was stirred at 650 rpm and irradiated under 300 W Xe lamp (λ = 320–780 nm). During the reaction, water was circulated to cool the reactor, keeping the temperature of the reactor at 40°C. To ensure the complete conversion of furfural in Figure 6, 50 mg of catalyst and 4 h of reaction time were adopted. For the conversions of 5-methlyfurfual and villain, the reaction

conditions were the same as those for the conversion of furfural in Figure 6 except for using reactant of 0.5 mmol and reaction time of 12 h. The light intensity was 600 mW cm^{-2} and the illumination area was 3.7 cm^2. After reaction, the solid catalyst was filtered and the products in the filtrate were identified by GC-MS and quantified by GC-FID and HPLC.

DFT Calculation

All the geometries were optimized using DFT as implemented in the freely available package CP2K/Quickstep.[54] For the reduced TiO_2 with excess electrons localizing at the surface Ti site next to bridge OH group, the redox potentials of Ti^{4+}/Ti^{3+} of the localized trapped electronic state obtained by using Perdew-Burke-Ernzerhof (PBE) density functional[55] and hybrid functional HSE06[56] are close.[57] Therefore, to alleviate computation time, the PBE functional with the Grimme's dispersion correction[58] was adopted. The Goedecker-Teter-Hutter (GTH) pseudopotentials[59] were used to represent the core electrons, and the double-ζ basis functions with one set of polarization functions (DZVP)[60] were employed to valence electrons. The atomic charges were calculated based on the Hirshfeld method.[61] Hirshfeld charge is considered to be the chemically meaningful charge[62] and is widely used in the charge-transfer analysis for adsorption system.[63,64] Further information on the computational setup in this work can be found in the Supplemental Information.

SUPPLEMENTAL INFORMATION

Supplemental Information can be found online at https://doi.org/10.1016/j.chempr.2020.08.014.

ACKNOWLEDGMENTS

This work was supported by the National Natural Science Foundation of China (nos. 21690082 and 21972115).

AUTHOR CONTRIBUTIONS

X.W. and S.X. performed most of the experiments and analyzed the experimental data; J.L. performed DFT computations and analyzed the computational data; P.D. and H.Z. synthesized TiO_2 semiconductors with different facets; J.F. performed a part of characterizations; Q.Z. analyzed all the data and co-wrote the paper; J.C. guided the computational work, analyzed all the data, and co-wrote the paper; Y.W. designed and guided the study, and co-wrote the paper; all of the authors discussed the results and reviewed the manuscript.

DECLARATION OF INTERESTS

The authors declare no competing interests.

Received: February 18, 2020
Revised: April 10, 2020
Accepted: August 18, 2020
Published: September 25, 2020

REFERENCES

1. Schneider, J., Matsuoka, M., Takeuchi, M., Zhang, J., Horiuchi, Y., Anpo, M., and Bahnemann, D.W. (2014). Understanding TiO_2 photocatalysis: mechanisms and materials. Chem. Rev. *114*, 9919–9986.

2. Henderson, M.A.A. (2011). A surface science perspective on TiO_2 photocatalysis. Surf. Sci. Rep. *66*, 185–297.

3. Liu, G., Yu, J.C., Lu, G.Q., and Cheng, H.M. (2011). Crystal facet engineering of semiconductor photocatalysts: motivations, advances and unique properties. Chem. Commun. (Camb.) *47*, 6763–6783.

4. Jing, L., Zhou, W., Tian, G., and Fu, H. (2013). Surface tuning for oxide-based nanomaterials

as efficient photocatalysts. Chem. Soc. Rev. *42*, 9509–9549.

5. Yang, H.G., Sun, C.H., Qiao, S.Z., Zou, J., Liu, G., Smith, S.C., Cheng, H.M., and Lu, G.Q. (2008). Anatase TiO_2 single crystals with a large percentage of reactive facets. Nature *453*, 638–641.

6. Ong, W.J., Tan, L.L., Chai, S.P., Yong, S.T., and Mohamed, A.R. (2014). Facet-dependent photocatalytic properties of TiO_2 -based composites for energy conversion and environmental remediation. ChemSusChem *7*, 690–719.

7. Kou, J., Lu, C., Wang, J., Chen, Y., Xu, Z., and Varma, R.S. (2017). Selectivity enhancement in heterogeneous photocatalytic transformations. Chem. Rev. *117*, 1445–1514.

8. Tu, W., Zhou, Y., and Zou, Z. (2014). Photocatalytic conversion of CO_2 into renewable hydrocarbon fuels: state-of-the-art accomplishment, challenges, and prospects. Adv. Mater. *26*, 4607–4626.

9. Colmenares, J.C., and Luque, R. (2014). Heterogeneous photocatalytic nanomaterials: prospects and challenges in selective transformations of biomass-derived compounds. Chem. Soc. Rev. *43*, 765–778.

10. Granone, L.I., Sieland, F., Zheng, N., Dillert, R., and Bahnemann, D.W. (2018). Photocatalytic conversion of biomass into valuable products: a meaningful approach? Green Chem. *20*, 1169–1192.

11. Wu, X., Fan, X., Xie, S., Lin, J., Cheng, J., Zhang, Q., Chen, L., and Wang, Y. (2018). Solar energy-driven lignin-first approach to full utilization of lignocellulosic biomass under mild conditions. Nat. Catal. *1*, 772–780.

12. Zhou, B., Song, J., Zhang, Z., Jiang, Z., Zhang, P., and Han, B. (2017). Highly selective photocatalytic oxidation of biomass-derived chemicals to carboxyl compounds over Au/TiO_2. Green Chem. *19*, 1075–1081.

13. Da Vià, L., Recchi, C., Gonzalez-Yañez, E.O., Davies, T.E., and Lopez-Sanchez, J.A. (2017). Visible light selective photocatalytic conversion of glucose by TiO_2. Appl. Catal. B *202*, 281–288.

14. Mariscal, R., Maireles-Torres, P., Ojeda, M., Sádaba, I., and López Granados, M. (2016). Furfural: a renewable and versatile platform molecule for the synthesis of chemicals and fuels. Energy Environ. Sci. *9*, 1144–1189.

15. Chen, S., Wojcieszak, R., Dumeignil, F., Marceau, E., and Royer, S. (2018). How catalysts and experimental conditions determine the selective hydroconversion of furfural and 5-hydroxymethylfurfural. Chem. Rev. *118*, 11023–11117.

16. Fache, M., Boutevin, B., and Caillol, S. (2016). Vanillin production from lignin and its use as a renewable chemical. ACS Sustainable Chem. Eng. *4*, 35–46.

17. Zang, H., Wang, K., Zhang, M., Xie, R., Wang, L., and Chen, E.Y.-X. (2018). Catalytic coupling of biomass-derived aldehydes into intermediates for biofuels and materials. Catal. Sci. Technol. *8*, 1777–1798.

18. Bond, J.Q., Alonso, D.M., Wang, D., West, R.M., and Dumesic, J.A. (2010). Integrated catalytic conversion of γ-valerolactone to liquid alkenes for transportation fuels. Science *327*, 1110–1114.

19. Gumidyala, A., Wang, B., and Crossley, S. (2016). Direct carbon-carbon coupling of furanics with acetic acid over brønsted zeolites. Sci. Adv. *2*, e1601072.

20. Wang, M., Liu, M., Lu, J., and Wang, F. (2020). Photo splitting of bio-polyols and sugars to methanol and syngas. Nat. Commun. *11*, 1083.

21. Zhang, J., and Chen, J. (2017). Selective transfer hydrogenation of biomass-based furfural and 5-hydroxymethylfurfural over hydrotalcite-derived copper catalysts using methanol as a hydrogen donor. ACS Sustain. Chem. Eng. *5*, 5982–5993.

22. Zhang, Z., Wang, C., Gou, X., Chen, H., Chen, K., Lu, X., Ouyang, P., and Fu, J. (2019). Catalytic in-situ hydrogenation of 5-hydroxymethylfurfural to 2,5-dimethylfuran over Cu-based catalysts with methanol as a hydrogen donor. Appl. Catal. A *570*, 245–250.

23. Luo, N., Montini, T., Zhang, J., Fornasiero, P., Fonda, E., Hou, T., Nie, W., Lu, J., Liu, J., Heggen, M., et al. (2019). Visible-light-driven coproduction of diesel precursors and hydrogen from lignocellulose-derived methylfurans. Nat. Energy *4*, 575–584.

24. Zhang, Y., Ding, Z., Foster, C.W., Banks, C.E., Qiu, X., and Ji, X. (2017). Oxygen vacancies evoked blue TiO_2(B) nanobelts with efficiency enhancement in sodium storage behaviors. Adv. Funct. Mater. *27*, 1700856.

25. Liu, L., Zhao, H., Andino, J.M., and Li, Y. (2012). Photocatalytic CO_2 reduction with H_2O on TiO_2 nanocrystals: comparison of anatase, rutile, and brookite polymorphs and exploration of surface chemistry. ACS Catal. *2*, 1817–1828.

26. Yang, Y., Yin, L.C., Gong, Y., Niu, P., Wang, J.Q., Gu, L., Chen, X., Liu, G., Wang, L., and Cheng, H.M. (2018). An unusual strong visible-light absorption band in red anatase TiO_2 photocatalyst induced by atomic hydrogen-occupied oxygen vacancies. Adv. Mater. *30*, 1704479.

27. Chen, X., Liu, L., Yu, P.Y., and Mao, S.S. (2011). Increasing solar absorption for photocatalysis with black hydrogenated titanium dioxide nanocrystals. Science *331*, 746–750.

28. Guo, Q., Zhou, C., Ma, Z., Ren, Z., Fan, H., and Yang, X. (2016). Elementary photocatalytic chemistry on TiO_2 surfaces. Chem. Soc. Rev. *45*, 3701–3730.

29. Fenoglio, I., Greco, G., Livraghi, S., and Fubini, B. (2009). Non-UV-induced radical reactions at the surface of TiO_2 nanoparticles that may trigger toxic responses. Chem. Eur. J. *15*, 4614–4621.

30. Sarkar, A., and Khan, G.G. (2019). The formation and detection techniques of oxygen vacancies in titanium oxide-based nanostructures. Nanoscale *11*, 3414–3444.

31. Yu, X., Kim, B., and Kim, Y.K. (2013). Highly enhanced photoactivity of anatase TiO_2 nanocrystals by controlled hydrogenation-induced surface defects. ACS Catal. *3*, 2479–2486.

32. Zhang, X., Tian, H., Wang, X., Xue, G., Tian, Z., Zhang, J., Yuan, S., Yu, T., and Zou, Z. (2013). The role of oxygen vacancy-Ti^{3+} states on TiO_2 nanotubes' surface in dye-sensitized solar cells. Mater. Lett. *100*, 51–53.

33. Fan, Y., Li, S., Bao, J., Shi, L., Yang, Y., Yu, F., Gao, P., Wang, H., Zhong, L., and Sun, Y. (2018). Hydrofunctionalization of olefins to value-added chemicals via photocatalytic coupling. Green Chem. *20*, 3450–3456.

34. Razzaq, A., Sinhamahapatra, A., Kang, T.H., Grimes, C.A., Yu, J.S., and In, S.I. (2017). Efficient solar light photoreduction of CO_2 to hydrocarbon fuels via magnesiothermally reduced TiO_2 photocatalyst. Appl. Catal. B *215*, 28–35.

35. Keulemans, M., Verbruggen, S.W., Hauchecorne, B., Martens, J.A., and Lenaerts, S. (2016). Activity versus selectivity in photocatalysis: morphological or electronic properties tipping the scale. J. Catal. *344*, 221–228.

36. Tian, J., Hu, X., Yang, H., Zhou, Y., Cui, H., and Liu, H. (2016). High yield production of reduced TiO_2 with enhanced photocatalytic activity. Appl. Surf. Sci. *360*, 738–743.

37. Sitthisa, S., Sooknoi, T., Ma, Y., Balbuena, P.B., and Resasco, D.E. (2011). Kinetics and mechanism of hydrogenation of furfural on Cu/SiO_2 catalysts. J. Catal. *277*, 1–13.

38. Lin, Y., Yan, Y., Peng, W., Qiao, X., Huang, D., Ji, H., Chen, C., Ma, W., and Zhao, J. (2020). Crucial effect of Ti—H species generated in the visible-light-driven transformations: slowed-down proton-coupled electron transfer. J. Phys. Chem. Lett. *11*, 3941–3946.

39. Xie, X.-Y., Xiao, P., Fang, W.-H., Cui, G., and Thiel, W. (2019). Probing photocatalytic nitrogen reduction to ammonia with water on the rutile TiO_2 (110) surface by first-principles calculations. ACS Catal. *9*, 9178–9187.

40. Meng, X., Ouyang, S., Kako, T., Li, P., Yu, Q., Wang, T., and Ye, J. (2014). Photocatalytic CO_2 conversion over alkali modified TiO_2 without loading noble metal cocatalyst. Chem. Commun. (Camb.) *50*, 11517–11519.

41. Schrauben, J.N., Hayoun, R., Valdez, C.N., Braten, M., Fridley, L., and Mayer, J.M. (2012). Titanium and zinc oxide nanoparticles are proton-coupled electron transfer agents. Science *336*, 1298–1301.

42. Xie, S., Shen, Z., Deng, J., Guo, P., Zhang, Q., Zhang, H., Ma, C., Jiang, Z., Cheng, J., Deng, D., and Wang, Y. (2018). Visible light-driven C-H activation and C-C coupling of methanol into ethylene glycol. Nat. Commun. *9*, 1181.

43. Li, Q.H., Gao, T., Wang, Y.G., and Wang, T.H. (2005). Adsorption and desorption of oxygen probed from ZnO nanowire films by photocurrent measurements. Appl. Phys. Lett. *86*, 123117.

44. Dolamic, I., and Bürgi, T. (2007). Photocatalysis of dicarboxylic acids over TiO_2: an in situ ATR-IR study. J. Catal. *248*, 268–276.

45. Babu, N.R., Subashchandrabose, S., Ali Padusha, M.S., Saleem, H., and Erdoğdu, Y. (2014). Synthesis and spectral characterization of hydrazone derivative of furfural using

experimental and DFT methods. Spectrochim. Acta A Mol. Biomol. Spectrosc. *120*, 314–322.

46. Xiong, K., Wan, W., and Chen, J.G. (2016). Reaction pathways of furfural, furfuryl alcohol and 2-methylfuran on Cu(111) and NiCu bimetallic surfaces. Surf. Sci. *652*, 91–97.

47. Thang, H.V., Tosoni, S., Fang, L., Bruijnincx, P., and Pacchioni, G. (2018). Nature of sintering-resistant, single-atom Ru species dispersed on zirconia-based catalysts: a DFT and FTIR Study of CO adsorption. ChemCatChem *10*, 2634–2645.

48. Luo, N., Hou, T., Liu, S., Zeng, B., Lu, J., Zhang, J., Li, H., and Wang, F. (2020). Photocatalytic coproduction of deoxybenzoin and H_2 through tandem redox reactions. ACS Catal. *10*, 762–769.

49. Nowotny, J., Alim, M.A., Bak, T., Idris, M.A., Ionescu, M., Prince, K., Sahdan, M.Z., Sopian, K., Mat Teridi, M.A., and Sigmund, W. (2015). Defect chemistry and defect engineering of TiO_2-based semiconductors for solar energy conversion. Chem. Soc. Rev. *44*, 8424–8442.

50. Li, H., Li, J., Ai, Z., Jia, F., and Zhang, L. (2018). Oxygen vacancy-mediated photocatalysis of BiOCl: reactivity, selectivity, and perspectives. Angew. Chem. Int. Ed. *57*, 122–138.

51. Liu, L., Jiang, Y., Zhao, H., Chen, J., Cheng, J., Yang, K., and Li, Y. (2016). Engineering coexposed {001} and {101} facets in oxygen-deficient TiO_2 nanocrystals for enhanced CO_2 photoreduction under visible light. ACS Catal. *6*, 1097–1108.

52. Han, X., Kuang, Q., Jin, M., Xie, Z., and Zheng, L. (2009). Synthesis of titania nanosheets with a high percentage of exposed (001) facets and related photocatalytic properties. J. Am. Chem. Soc. *131*, 3152–3153.

53. Zhang, J., Liu, P., Lu, Z., Xu, G., Wang, X., Qian, L., Wang, H., Zhang, E., Xi, J., and Ji, Z. (2015). One-step synthesis of rutile nano-TiO_2 with exposed {111} facets for high photocatalytic activity. J. Alloys Compd. *632*, 133–139.

54. VandeVondele, J., Krack, M., Mohamed, F., Parrinello, M., Chassaing, T., and Hutter, J. (2005). Quickstep: fast and accurate density functional calculations using a mixed Gaussian and plane waves approach. Comput. Phys. Commun. *167*, 103–128.

55. Perdew, J.P., Burke, K., and Ernzerhof, M. (1996). Generalized gradient approximation made simple. Phys. Rev. Lett. *77*, 3865–3868.

56. Krukau, A.V., Vydrov, O.A., Izmaylov, A.F., and Scuseria, G.E. (2006). Influence of the exchange screening parameter on the performance of screened hybrid functionals. J. Chem. Phys. *125*, 224106.

57. Cheng, J., Liu, X., VandeVondele, J., and Sprik, M. (2015). Reductive hydrogenation of the aqueous rutile TiO_2 (110) surface. Electrochim. Acta *179*, 658–667.

58. Grimme, S., Antony, J., Ehrlich, S., and Krieg, H. (2010). A consistent and accurate ab initio parametrization of density functional dispersion correction (DFT-D) for the 94 elements H-Pu. J. Chem. Phys. *132*, 154104.

59. Hartwigsen, C., Goedecker, S., and Hutter, J. (1998). Relativistic separable dual-space Gaussian pseudopotentials from H to Rn. Phys. Rev. B *58*, 3641–3662.

60. VandeVondele, J., and Hutter, J. (2007). Gaussian basis sets for accurate calculations on molecular systems in gas and condensed phases. J. Chem. Phys. *127*, 114105.

61. Hirshfeld, F.L. (1977). Bonded-atom fragments for describing molecular charge densities. Theor. Chim. Acta *44*, 129–138.

62. Fonseca Guerra, C., Handgraaf, J.W., Baerends, E.J., and Bickelhaupt, F.M. (2004). Voronoi deformation density (VDD) charges: assessment of the Mulliken, Bader, Hirshfeld, Weinhold, and VDD methods for charge analysis. J. Comput. Chem. *25*, 189–210.

63. Jiang, Y., Adams, J.B., and Sun, D. (2004). Benzotriazole adsorption on Cu_2O (111) surfaces: a first-principles study. J. Phys. Chem. B *108*, 12851–12857.

64. Watanabe, T., Manz, T.A., and Sholl, D.S. (2011). Accurate treatment of electrostatics during molecular adsorption in nanoporous crystals without assigning point charges to framework atoms. J. Phys. Chem. C *115*, 4824–4836.